ASEAN
Journal of Scientific and Technological Reports
Online ISSN:2773-8752

Research article

Electron Spin Resonance (ESR) Signal Analysis of Fossil Teeth from Mae Moh Mine, Thailand

Tidarut Vichaidid[1*], and Sumaiyah Kortor[1]

[1] Faculty of Science and Technology, Prince of Songkla University, Pattani Campus, Pattani, 94000, Thailand
* Correspondence: tidarut.v@psu.ac.th

Citation:
Vichaidid, T.; Kortor, S. Electron spin resonance (ESR) signal analysis of fossil teeth from Mae Moh Mine, Thailand. *ASEAN J. Sci. Tech. Report.* **2026**, *29*(3), e260951. https://doi.org/10.55164/ajstr.v29i3.260951.

Article history:
Received: August 21, 2025
Revised: January 26, 2026
Accepted: February 5, 2026
Available online: February 28, 2026

Abstract: This study investigates the characteristics of Electron Spin Resonance (ESR) signals in fossil tooth enamel collected from the Mae Moh lignite mine in Lampang Province, Thailand. ESR spectra were recorded at room temperature (298 K) using a Bruker EMX Premium spectrometer operating at X-band (9.85 GHz) with a modulation frequency of 100 kHz and a modulation amplitude of 0.3 mT. The most prominent signal was observed at g ≈ 2.002, attributable to trapped carbonate radicals within the hydroxyapatite crystal lattice. By applying the Multiple-Aliquot Additive Dose (MAAD) protocol, the ESR intensity at g ≈ 2.002 exhibited a strong linear relationship with laboratory-administered gamma doses (0–2000 Gy), yielding a dose-response slope of 0.2185 a.u./Gy (R^2 = 0.907). From this calibration, the natural accumulated dose for the fossil teeth was determined to be 550 ± 30 Gy. These findings demonstrate the reliability of ESR signal analysis for quantifying accumulated radiation dose in fossil enamel and support its application for future geochronological investigations in the Mae Moh basin.

Keywords: ESR signal intensity; fossil tooth enamel; multiple-aliquot additive dose (MAAD); accumulated dose

1. Introduction

Electron Spin Resonance (ESR) spectroscopy is a powerful analytical method for detecting unpaired electrons and free radicals in paramagnetic materials, offering high sensitivity and specificity [1]. It has been extensively applied in archaeometry and geosciences to characterize fossil, bone, and tooth samples and to assess radiation-induced defect centers [2]. Tooth enamel, composed primarily of hydroxyapatite $(Ca_{10}(PO_4)_6(OH)_2)$ and organic inclusions, undergoes structural defect formation and radical entrapment during prolonged burial. The most prominent ESR-active center in fossil enamel is the carbonate radical (CO_2^-), which produces a characteristic signal at g ≈ 2.002, making it an ideal probe for dosimetric and microstructural studies [3]. The Mae Moh lignite mine in Lampang Province, Thailand, is a key Miocene depositional basin (15–20 Ma) known for abundant mammalian fossils, including well-preserved tooth and bone specimens. This geological context offers a unique archive of diagenetic processes and paleoenvironmental conditions in northern Thailand [4]. ESR-based dosimetry and dating commonly employ the MAAD protocol to calibrate signal intensity against known $\gamma-$ray doses. Standardized procedures, as outlined by Dennis [5] and Said et al. [6], ensure reliable assessment of accumulated radiation doses in enamel, providing groundwork for subsequent

age estimation. This study presents a detailed analysis of ESR signals in fossil tooth enamel from the Mae Moh mine, focusing on signal amplitude, line shape, and the precise determination of the g ≈ 2.002 component. We establish a dose–response calibration, derive the natural accumulated dose, and evaluate the potential of ESR signal analysis for paleodosimetric applications and future geochronological research in the Mae Moh basin [6].

2. Materials and Methods

2.1 Study Area and Sample Collection

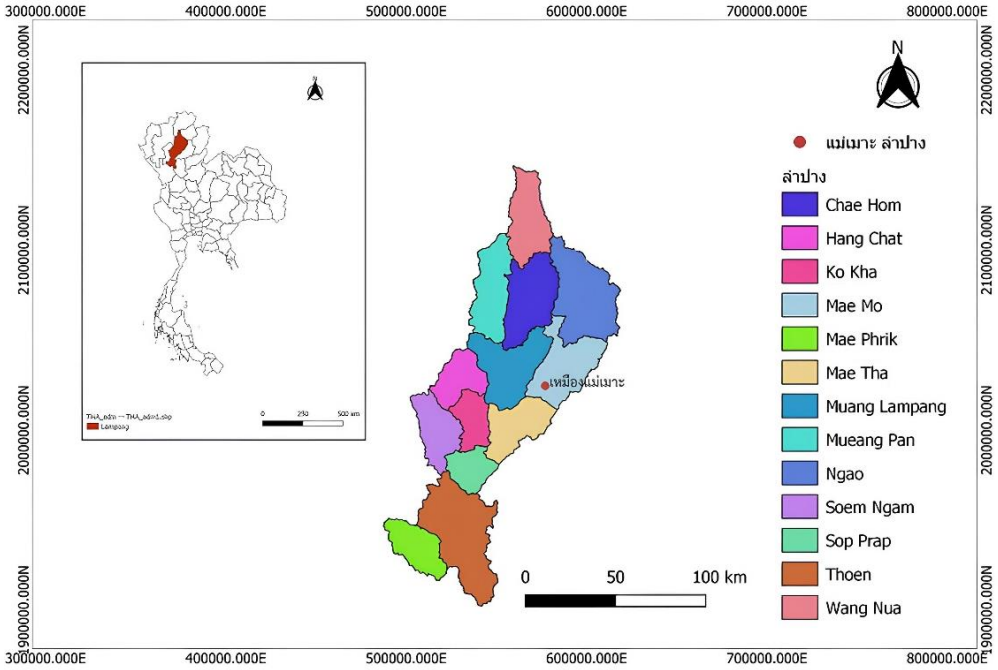

Figure 1. Map of the Mae Moh lignite mine showing sampling locations (red dots) within the Miocene graben basin [7-8].

The study was conducted in the Mae Moh lignite mine (18°20′–18°27′ N, 99°40′–99°46′ E) in Lampang Province, northern Thailand (Figure 1). This mine lies within the Miocene Mae Moh Graben Basin, a fault-bounded depression with more than 1,000 m of fluvio-lacustrine sediments that have yielded diverse vertebrate fossils [7]. The stratigraphy of the Mae Moh Group comprises three lithostratigraphic members—Huai King, Nakhaem, and Huai Luang—each characterized by alternating coal seams and clastic units (Figure 2) [7]. Fossil tooth enamel specimens were discovered in the Nakhaem member, specifically within the interburden between coal seams K-3 and K-4, at an elevation of approximately 332 m above sea level and beneath ~18 m of overburden (Figure 3). Field sampling followed established ESR-dating guidelines: GPS coordinates, stratigraphic position, overburden thickness, and sedimentological context were recorded at each find [9]. To prevent photobleaching of trapped radicals, each tooth was immediately wrapped in opaque aluminum foil and stored under dim red light (<5 lx) until laboratory processing [9-10].

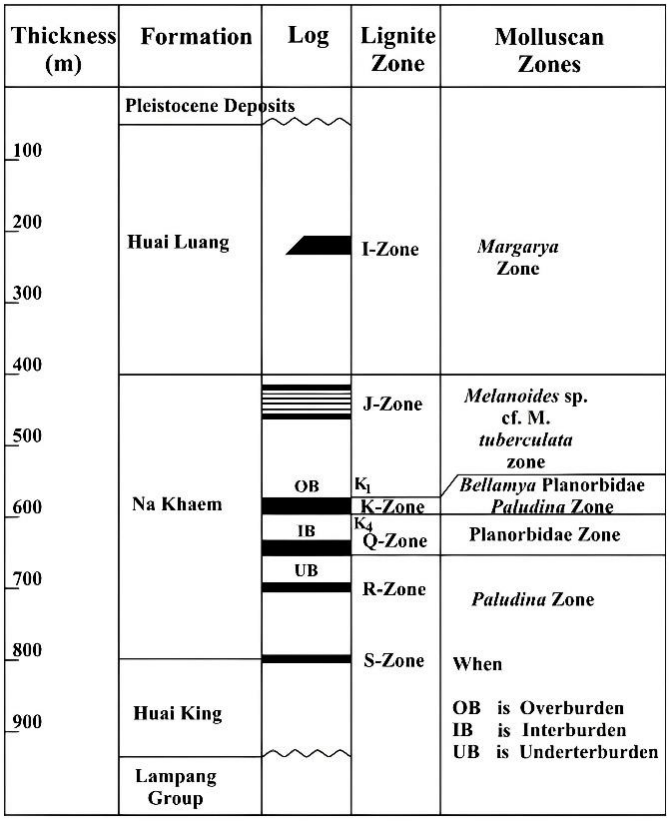

Figure 2. Simplified stratigraphic column of the Mae Moh Group, indicating the Huai King, Nakhaem, and Huai Luang members with fossil-bearing horizons between coal seams K-3 and K-4 [7].

Figure 3. Fossil molar tooth recovered from the sediment between coal seams K-3 and K-4 at the Mae Moh lignite mine, Lampang Province, Thailand, showing the occlusal surface. (scale bar = 1 cm).

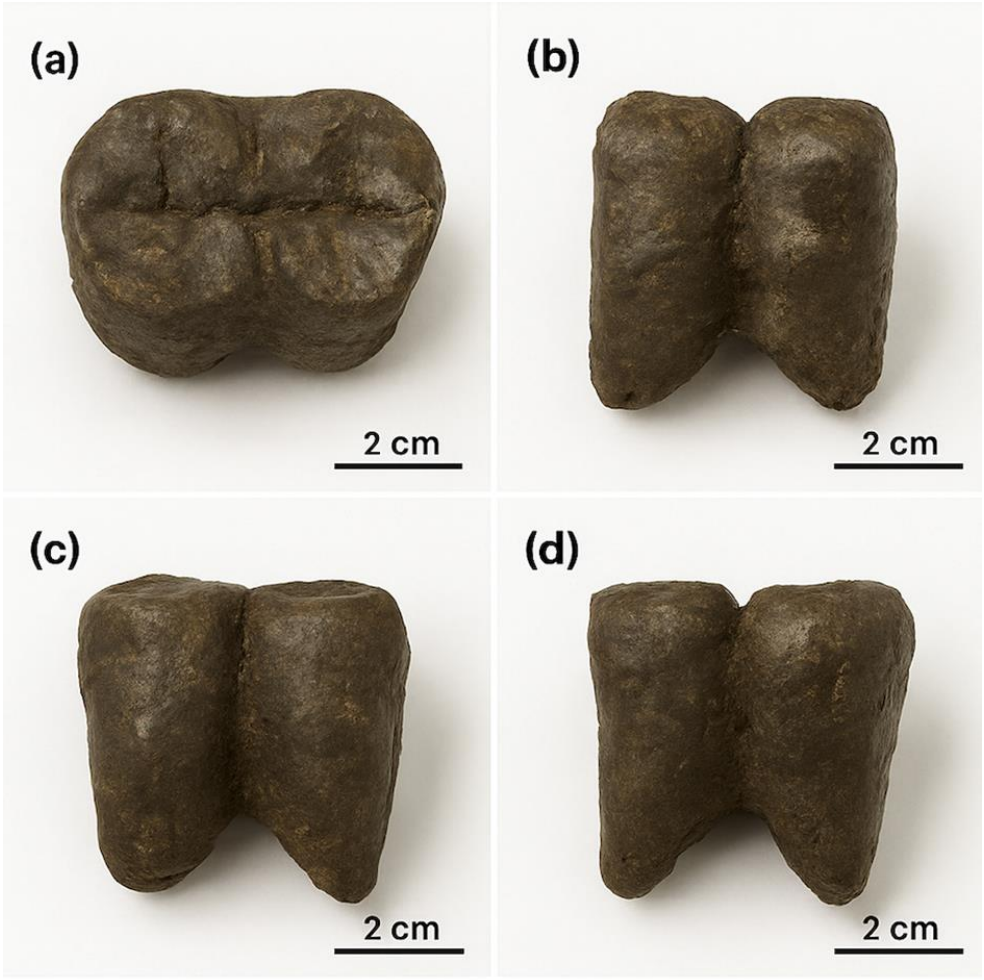

Figure 4. Simulated four-view presentation of the fossilized molar tooth pair recovered from the member (between coal seams K-3 and K-4) at the Mae Moh lignite mine, Lampang Province, Thailand. Panels show (a) occlusal surface, (b) frontal aspect, (c) buccal aspect, and (d) distal aspect. Scale bars = 2 cm. This illustration was digitally generated for illustrative purposes and does not depict the actual specimen.

2.2 Sample Preparation

To preserve the radicals formed during burial, freshly excavated fossil teeth were wrapped in light-proof foil and stored under dim red light (<5 lx) until laboratory preparation. In the laboratory, the enamel layer was separated from dentine under red light and processed for ESR measurements. The surrounding sediment does not alter the spectral shape or intensity of the ESR signal in enamel, as the detected ESR response reflects the concentration and stability of trapped paramagnetic centers within the hydroxyapatite lattice, which are primarily governed by the cumulative radiation dose and defect structure of the enamel. Therefore, sediment analyses were not considered within the scope of this study, which focuses on ESR signal characterization rather than external dose-rate modeling. The outer ~3 mm was removed following International Atomic Energy Agency (IAEA) recommendations [11]. The resulting powder (90–150 μm) was obtained by gentle crushing and sieving. Chemical etching was not performed to avoid alteration of trapped radicals, in agreement with studies showing minimal benefit of additional HF treatment for ESR signals in well-preserved samples [9, 12].

2.3 ESR Measurements

Before measurement, powdered enamel (90–150 μm) was transferred into quartz ESR tubes and rinsed sequentially in 48 % HF (60 min), 10 % HCl, deionized water, and acetone to remove residual silicates and organic matter. Spectra were acquired at room temperature (298 K) on a Bruker EMX Premium X-band spectrometer (9.85 GHz) fitted with a high-Q dielectric cavity. Instrument settings were optimized to maximize signal-to-noise while avoiding power saturation: microwave power = 0.1002 mW, modulation frequency = 100 kHz, modulation amplitude = 0.3 mT, sweep width = 20 mT, center field = 351 mT, sweep time = 10.51 s, and a single scan per aliquot. Each spectrum was baseline-corrected and normalized using the manufacturer's software, and the g ≈ 2.002 carbonate radical signal was verified by comparison with a standard tooth-enamel reference [3]. Reproducibility was confirmed by repeated measurements (n = 3) on selected samples, yielding intensity variations below 5 % [13]. These procedures follow best practices for ESR dosimetry in enamel as outlined by Formela [1] and Viorel et al. [14].

2.4 Data Analysis

All ESR spectra were first subjected to baseline correction and a five-point moving-average smoothing using Bruker Xenon software to remove low-frequency noise and enhance the signal-to-noise ratio [15]. The CO_2^- signal at g ≈ 2.002 was isolated by spectral deconvolution employing Maximum Likelihood Common Factor Analysis (MLCFA), following the procedure of [15]. Peak-to-peak amplitudes were determined by integrating the first-derivative line shape between 350.9 and 352.0 mT.

The g-factor for each spectrum was calculated as

$$g = h\nu / \mu_B B \quad (1)$$

where h is Planck's constant, ν the microwave frequency, μ_B the Bohr magneton, and B the magnetic field at resonance. Dose–response curves were constructed by plotting integrated signal intensities against administered $\gamma-$ray doses (0–2000 Gy) and fitting a weighted linear regression constrained through the origin to obtain the calibration slope and coefficient of determination (R^2) [15]. To quantify uncertainty, we evaluated contributions from spectral noise, dose delivery (±2%), and regression fitting. Combined standard uncertainties and 95% confidence intervals for the natural accumulated dose were calculated using the analytical framework of Ahn et al. [16], which propagates error sources through dose determination to yield interval estimates rather than single values.

3. Results and Discussion

3.1 ESR Signal Characteristics

The room-temperature X-band ESR spectrum of fossil tooth enamel from the Mae Moh mine (Figure 5) is characterized by a sharp, single-component line centered at g ≈ 2.002, attributable to the CO_2^- in the hydroxyapatite lattice [17-18]. This narrow line (peak-to-peak width ≈ 0.6 mT) indicates a homogeneous microenvironment around the radical sites and minimal spectral overlap with other defect centers [19]. Recent advances in ESR spectral processing [17] have improved deconvolution accuracy, confirming that the CO_2^- signal dominates the spectrum with reproducibility better than 5% across multiple scans. Carbonate radicals form when the environment liberates electrons that become trapped in lattice vacancies during prolonged burial and diagenesis. Their geological stability and linear dose–response make the g ≈ 2.002 signal an ideal dosimetric marker for retrospective dose assessment in enamel [18].

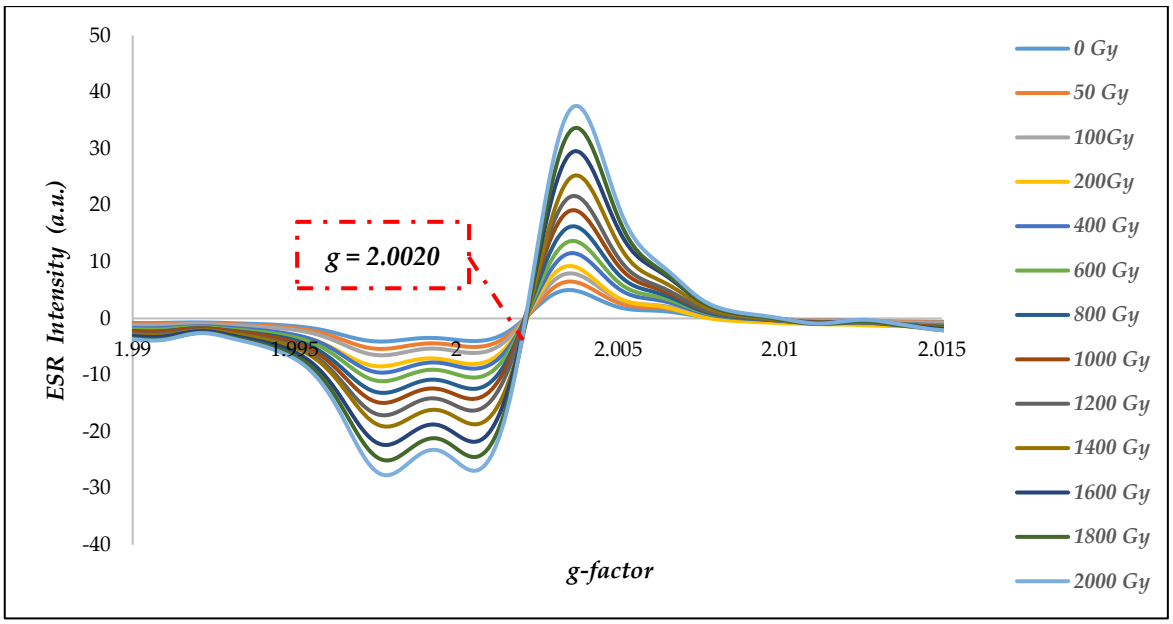

Figure 5. X-band ESR spectrum (first-derivative) of fossil tooth enamel from Mae Moh mine at 298 K, showing the dominant CO_2^- radical signal at g ≈ 2.002 (peak-to-peak width ≈ 0.6 mT)—inset: deconvoluted line shape used for amplitude extraction.

3.2 ESR Signal Intensity

The peak-to-peak ESR intensity of the CO_2^- signal at g ≈ 2.002 shows a strong linear relationship with administered $\gamma-$ray doses from 0 to 2000 Gy (Figure 6). A weighted linear regression constrained through the origin yields a calibration slope of 0.2185 ± 0.005 a.u./Gy and a coefficient of determination (R^2) of 0.9066, indicating that over 90% of the variance in signal intensity is explained by the applied dose. The y-intercept (120.49 a.u.) reflects the background contribution from intrinsic paramagnetic centers and instrument baseline; this offset is subtracted from all measured intensities before dose calculation. From this calibration, the natural accumulated dose (AD) in the fossil enamel is determined to be 550 ± 30 Gy. The uncertainty was derived by propagating three main error sources—spectral noise, dose-delivery error (±2%), and regression fitting uncertainty—using the analytical framework of viorel et at. [14] and Ahn et al. [16]. These results demonstrate that ESR intensity measurements provide a reliable and quantitative basis for retrospective dose assessment in tooth enamel, underpinning future paleodosimetric and geochronological applications.

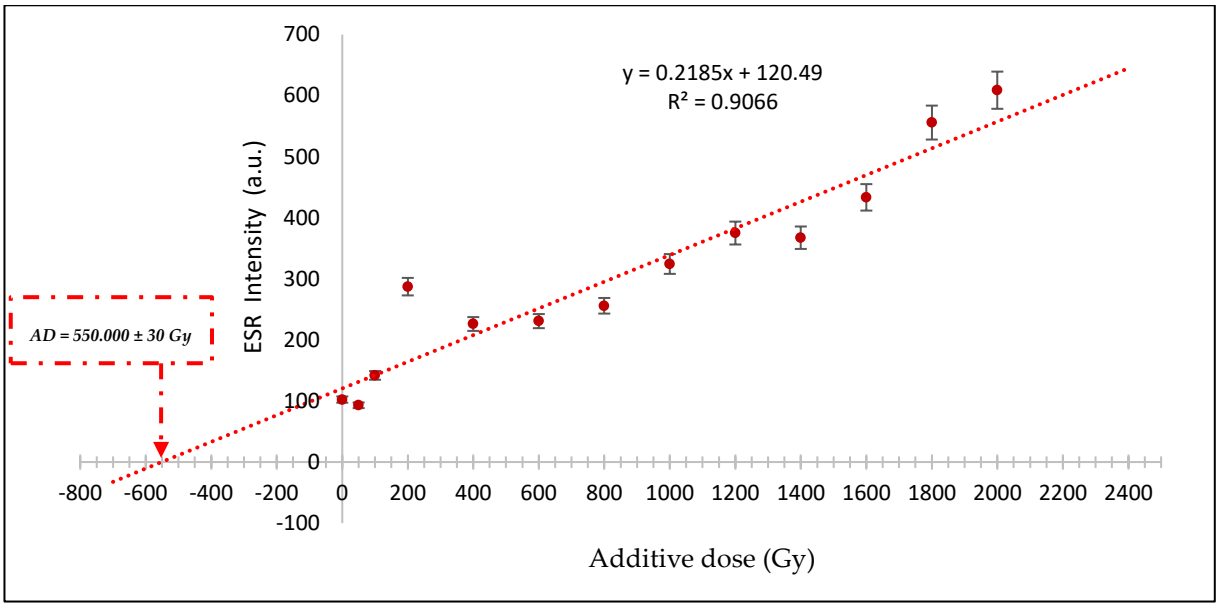

Figure 6. Dose–response calibration for the CO_2^- ESR signal at g ≈ 2.002 in fossil tooth enamel. The dashed line represents the weighted linear regression (slope = 0.2185 a.u./Gy; R^2 = 0.9066). The extrapolated natural accumulated dose is 550 ± 30 Gy.

3.3 Limitations and Potential Applications

While the MAAD protocol offers a robust approach for reconstructing accumulated dose (AD) from ESR measurements on fossil enamel, several methodological limitations remain. The accuracy of AD estimation depends on the quality of the dose–response curve and the reproducibility of the carbonate radical signal at g ≈ 2.002, which may vary among fossil specimens and diagenetic settings [5]. In addition, the lack of a complete external dose-rate model in the present study prevents AD values from being converted into numerical age estimates, as ESR dating requires integrating both internal and external radiation components, including sediment radioelements and moisture content [6, 22]. Analytical uncertainties related to spectral noise, dose delivery, and regression fitting must also be considered when interpreting AD results [14]. Despite these limitations, ESR enamel dosimetry holds promising applications in radiation and geochronological research. In palaeodosimetry, ESR signal intensities provide a direct proxy for long-term environmental radiation exposure in biological tissues and complement other retrospective dosimetry techniques [20]. Furthermore, ESR-based AD values can be integrated with U-series or luminescence chronometers to cross-validate burial ages and refine Quaternary stratigraphic frameworks [6]. Continued methodological improvements in signal processing, dose-response modeling, and dose-rate assessment will further enhance the utility of ESR enamel dosimetry in geochronological and radiation exposure studies.

4. Conclusions

This study demonstrates that fossil tooth enamel from the Mae Moh lignite mine exhibits a remarkably stable ESR signal at g ≈ 2.002, characterized by a narrow peak-to-peak width (~0.6 mT) and highly reproducible intensities across additive doses up to 2000 Gy, yielding a linear dose–response calibration (slope = 0.2185 a.u./Gy, R^2 = 0.9066) and a natural accumulated dose of 550 ± 30 Gy. The persistence and sharpness of this g ≈ 2.002 signal reflect the deep-trap stability of the CO_2^- center within the carbonated hydroxyapatite lattice, which has been shown to retain its paramagnetic properties with less than 4% signal variation over 360 days in analogous synthetic systems [2] and to resist diagenetic alteration in natural enamel samples [20]. Future research should prioritize refining environmental dose-rate models through comprehensive field-based measurements of radionuclide concentrations (U, Th, K) and sediment moisture content, enabling accurate quantification of both internal and external dose-rate components [5, 21]. Coupling these geochemical datasets with advanced MAAD protocols will improve the precision of ESR calibration curves. At the same time,

integration of ESR-derived doses with complementary chronometers—such as U-series and luminescence dating—will allow cross-validation of age estimates and the construction of a robust multi-method geochronological framework [22]. This integrated approach promises high-resolution reconstructions of Miocene sedimentation dynamics and vertebrate evolutionary history in northern Thailand.

5. Acknowledgements

The authors wish to express their sincere gratitude to the Department of Mineral Resources for its invaluable assistance in conducting field surveys and collecting samples at the Mae Moh mine in Lampang Province. We are also grateful to the National Standard Radiation Laboratory (NSRL), Office of Atoms for Peace (OAP), for providing the gamma irradiation support and for kindly granting access to the Electron Spin Resonance instrumentation. Finally, we would like to thank the Nuclear Physics Laboratory, Faculty of Science and Technology, Prince of Songkla University, Pattani Campus, for generously allowing us to use their research facilities.

Author Contributions: Conceptualization, Tidarut Vichaidid and Sumaiyah Kortor; methodology, Tidarut Vichaidid and Sumaiyah Kortor; software, Tidarut Vichaidid; validation, Tidarut Vichaidid; formal analysis, Tidarut Vichaidid; investigation, Tidarut Vichaidid; resources, Tidarut Vichaidid; data curation, Tidarut Vichaidid; writing—original draft preparation, Tidarut Vichaidid and Sumaiyah Kortor; writing—review and editing, Tidarut Vichaidid; visualization, Tidarut Vichaidid; supervision, Tidarut Vichaidid; project administration, Tidarut Vichaidid. All authors have read and agreed to the published version of the manuscript.

Funding: This research received no external funding

Conflicts of Interest: The authors declare no conflict of interest.

References

[1] Formela, K. Waste tire rubber-based materials: Processing, performance properties and development strategies. *Adv. Ind. Eng. Polym. Res.* **2022**, *5*(4), 234–247. https://doi.org/10.1016/j.aiepr.2022.06.003

[2] Ali, F.; Denis, R. Waste Rubber Recycling: A Review on the Evolution and Properties of Thermoplastic Elastomers. *Materials* **2020**, *13*(3), 782. https://doi.org/10.3390/ma13030782

[3] Daniele, R.; Andrea, D. Novel uses of recycled rubber in civil applications. *Adv. Ind. Eng. Polym. Res.* **2022**, *5*(4), 214–233. https://doi.org/10.1016/j.aiepr.2022.08.005

[4] Pranay, G.; Sukhanand, S. B.; Rohit, S.; Praful, S.; Ajay, G. D. Use of waste rubber tyre in construction of bituminous road. *Int. Res. J. Mod. Eng. Technol. Sci.* **2023**, *5*(8), 1395–1401. https://doi.org/10.56726/irjmets44098

[5] Dennis, G. The value of different recycling technologies for waste rubber tires in the circular economy—A review. *Front. Sustain.* **2024**, *4*, 1282805. https://doi.org/10.3389/frsus.2023.1282805

[6] Said, S.; Lucía, A.; Morena, R. M.; Nourredine, A. H. Thermo-mechanical devulcanization and recycling of rubber industry waste. *Resour. Conserv. Recycl.* **2019**, *144*, 180–186. https://doi.org/10.1016/j.resconrec.2019.01.047

[7] Zhao, X.; Hu, H.; Zhang, D.; Zhang, Z.; Peng, S.; Sun, Y. Curing behaviors, mechanical properties, dynamic mechanical analysis and morphologies of natural rubber vulcanizates containing reclaimed rubber. *e-Polymers* **2019**, *19*(1), 482–488. DOI: 10.1515/epoly-2019-0051

[8] Darestani, F. T.; Bakhshandeh, G. R.; Abtahi, M. Mechanical and Viscoelastic properties of natural rubber/reclaimed rubber blends. *Polym. Bull.* **2006**, *56*(4-5), 495–505. https://doi.org/10.1007/s00289-006-0508-4

[9] Aditya, R.; Pranav, K. S.; Prashant, P.; Nimisha, R. S. Minimization and Utilization of Byproduct. *Int. J. Innov. Eng. Sci.* **2023**, *8*(5), 38–41. https://doi.org/10.46335/IJIES.2023.8.5.8

[10] Mishel, P. F.; Steffi, P. F.; Vijayalakshmi, S. Conventional and modern waste treatment approaches – bioremediation of rubber waste. In *Sustainable Bio-Remediation of Waste Rubber*, Elsevier: **2023**; pp 97–113. https://doi.org/10.1016/B978-0-443-15206-1.00007-4

[11] Tao, Z.; Lucia, A.; Michel, G.; Nourredine, A. H. An overview on waste rubber recycling by microwave devulcanization. *J. Environ. Manage.* **2024**, *353*, 120122. https://doi.org/10.1016/j.jenvman.2024.120122.

[12] Woo, C. S.; Park, H. S. Useful lifetime prediction of rubber component. *Eng. Fail. Anal.* **2011**, *18*(7), 1645–1651. https://doi.org/10.1016/j.engfailanal.2011.01.003

[13] Núñez, L.; Villanueva, M.; Núñez, M. R.; Rial, B. Lifetime prediction of the epoxy system DGEBA (n= 0)/1, 2-DCH modified with an epoxy reactive diluent by thermogravimetric analysis. *J. Appl. Polym. Sci.* **2003**, *89*(14), 3835–3839. https://doi.org/10.1002/app.12536

[14] Viorel, S.; Orsina, V.; Alexandru, P. The estimation of thermal endurance for some heteropoly acidic catalysts from thermogravimetric decomposition data. *J. Therm. Anal. Calorim.* **2017**, *127*(1), 273–282. https://doi.org/10.1007/s10973-016-5479-6

[15] Ngudsuntear, K.; Limtrakul, S.; Vatanatham, T.; Arayapranee, W. Mechanical and aging properties of hydrogenated epoxidized natural rubber and its lifetime prediction. *ACS Omega* **2022**, *7*(41), 36448–36456. https://doi.org/10.1021/acsomega.2c04225

[16] Ahn, W.; Lee, J. M.; Lee, H. S. A Study on Life Time Prediction of ACM Rubber Composite Using Accelerated Test and Thermogravimetric Analysis. *Elastomers Compos.* **2014**, *49*(2), 144–148. https://doi.org/10.7473/EC.2014.49.2.144

[17] Toop, D. Theory of Life Testing and Use of Thermogravimetric Analysis to Predict the Thermal Life of Wire Enamels. *IEEE Trans. Electr. Insul.* **1971**, *EI-6*(1), 2–14. https://doi.org/10.1109/TEI.1971.299128.

[18] Plota, A.; Masek, A. Lifetime Prediction Methods for Degradable Polymeric Materials—A Short Review. *Materials* **2020**, *13* (20), 4507. DOI: 10.3390/ma13204507

[19] Saiwari, S.; Lohyi, E.; Nakason, C. Application of NR Gloves Reclaim: Cure and Mechanical Properties of NR/Reclaim Rubber Blends. *Adv. Mater. Res.* **2013**, *844*, 437–440. https://doi.org/10.4028/www.scientific.net/AMR.844.437

[20] Thitithammawong, A.; Hayichelaeh, C.; Nakason, W.; Jehvoh, N. The use of reclaimed rubber from waste tires for production of dynamically cured natural rubber/reclaimed rubber/polypropylene blends: Effect of reclaimed rubber loading. *J. Met. Mater. Miner.* **2019**, *29*(2), 85–94. https://doi.org/10.14456/jmmm.2019.24

[21] Candau, N.; Chazeau, L.; Chenal, J. M.; Gauthier, C.; Ferreira, J.; Munch, E.; Thiaudière, D. Strain induced crystallization and melting of natural rubber during dynamic cycles. *Phys. Chem. Chem. Phys.* **2015**, *17* (23), 15331–15338. https://doi.org/10.1039/C5CP00384A

[22] Lu, L.; Lu, L.; Cai, J.; Frost, R. L. Desorption of stearic acid upon surfactant adsorbed montmorillonite: A thermogravimetric study. *J. Therm. Anal. Calorim.* **2010**, *100*(1), 141–144. https://doi.org/10.1007/s10973-009-0169-2

[23] Ammineni, S. P.; Nagaraju, C.; Lingaraju, D. Thermal degradation of naturally aged NBR with time and temperature. *Mater. Res. Express* **2022**, *9*(6), 065305. https://doi.org/10.1088/2053-1591/ac7302.

[24] Mohit, A.; Remya, N. Pyrolysis characteristics and kinetics study of native polyculture microalgae using thermogravimetric analysis. *Biomass Convers. Biorefin.* **2024**, *14*(16), 19825–19833. https://doi.org/10.1007/s13399-023-04175-z

[25] Joseph, A. M.; George, B.; Alex, R. Effect of devulcanization on crosslink density and crosslink distribution of carbon black filled natural rubber vulcanizates. *Rubber Chem. Technol.* **2016**, *89*(4), 653–670. https://doi.org/10.5254/rct.16.84819